ISSN 1392-1207. MECHANIKA. Vol. 32, No. 1, 2026: 49–55

The Structure Design and Precision Improvement of Small Caliber Non-Spherical Surface Type Detector

Yan LI*, Yue HU, Bo YU*****

**School of Mechanical and Electrical Engineer, Changchun Institute of Technology, Changchun, Jilin 130012, China*

***College of Physics and Electronic Engineering, Hebei Minzu Normal University, Chengde, Hebei 067000, China, E-mail: jdhy@hbun.edu.cn (Corresponding Author)*

****School of Mechanical and Electrical Engineer, Changchun Institute of Technology, Changchun, Jilin 130012, China*

https://doi.org/10.5755/j02.mech.42129

1. Introduction

With the rapid development of modern optical technology, aspheric optical elements have been widely used in aerospace, laser communication, astronomical observation, medical imaging and other fields their excellent optical performance [1, 2].

Compared with traditional spherical elements, non-spherical surface types can effectively correct a variety of aberrations, significantly improving the imaging quality and energy utilization of systems. However, the complexity of non-spherical curvature and the high-precision machining requirements make its surface shape detection a bottleneck problem that restricts its application [3,4].

Especially under the background of the booming development of precision manufacturing technology, the precision, efficiency and cost control of surface shape measurement of small-aperture nonspherical elements are put forward with more stringent requirements due to their critical role in high-resolution imaging systems and photonics devices.

At present, the main technical means of non-spherical surface shape detection include contact contour meter [5], interferometric method [6], self-collimation projection detection [7]. Among them, contact measurement is easily affected by probe wear and has low efficiency; although interferometry can achieve sub-nanometer, it is sensitive to environmental vibration and needs high-precision standard parts, so it is difficult to achieve full-aperture rapid detection of small-aperture non-heres; And the self-collimation projection technology based on machine vision has contactless advantages, but its measurement accuracy is often limited by the aberration of the optical system environmental disturbances. Therefore, it is of great engineering value to develop a high-precision, strong anti-interference and low-cost small-aperture non-sp special detection device.

In view of the above challenges, this research focuses on the structural design and precision optimization of small-caliber aspheric surface instruments. An innovative detection for small-caliber aspheric surface shape based on the theory of the closest circle is proposed, aiming to break through the limitations of traditional detection methods. The key points of this include: 1. In-depth analysis of the detection principle of aspheric surface shape based on the theory of the closest circle; 2. Overall structural design of small-iber aspheric surface instrument; 3. Proposal of compensation scheme for geometric error of small-caliber aspheric surface instrument; 4. Construction of mathematical model for implementation of geometric error compensation of small-caliber aspheric surface instrument; 5. Implementation of comprehensive full compensation of geometric error of small-caliber aspheric surface instrument, and advanced nature of the research content is verified, providing theoretical support and technical path for the independent research and development of domestic high-end optical detection equipment.

2. Principle Analysis of Detection

In the detection of aspheric elements, how to measure the deviation amount of the aspheric surface shape from the closest sphere and then compare its design value with the difference value closest to the sphere is an important content of aspheric detection [8].

2.1. Principle of detection

In this study, a new principle for the detection of non-spherical surface profiles is conceived, as shown in Fig. 1, where the OP_iP_{max} is the theoretical contour line of the non-spherical element to be detected, the curve $OP_i'P_{max}$ is the line of the nearest sphere of the-spherical surface to be detected, O' is the center of the sphere of the nearest sphere, R is the radius of the nearest sphere, P_i is an arbitrary point on theoretical contour line of the non-spherical surface, and P_i' is a point on the line $O'P_i$ extended to the nearest point on the circle.

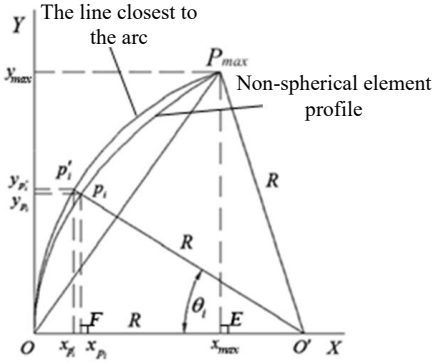

Fig. 1 Schematic diagram of detection principle

If the circle is at O' and the difference $P_i'P_i$ between the non-spherical theoretical trajectory OP_iP_{max} and the nearest circle $OP_i'P_{max}$ is used as the measurement benchmark the non-spherical surface is rotated in real time to achieve real-time measurement of the difference between

the actual trajectory of the non-spherical surface and the nearest circle, comparing and checking the two data, then the surface profile error of the measured non-spherical surface can be obtained, which is the basic principle of the nearest circle method to achieve detection of non-spherical surface profiles.

2.2. Implementation of detection

The characteristic of the spherical surface is that it has innumerable axes of symmetry and its contour is determined by the radius of the spherical surface; the non-sp surface corresponding to the spherical surface refers to the surface that only has one axis of rotational symmetry and the contour of the surface is determined by many parameters, and its curve equation is expressed Eq. (1):

$$x = \frac{cy^2}{1+\sqrt{1-(k+1)c^2y^2}} + Ay^4 + By^6 + \ldots . \quad (1)$$

In Eq. (1), c is the non-spherical vertex radius of curvature; k is the quadratic curve constant; and A, B, … are the coefficients of the higher-order terms of the non-spherical surface. If the size of the non-spherical surface is known, then its aperture D is.

For the tested element, in order to detect its surface shape error, the equation of the curve should be known first, as shown in Eq. (1). Parameters c, k, A, B of the tested element should be known, and the size of the caliber D of the tested element should be known. From the caliber D of tested element, the maximum value of the Y direction of the tested element can be determined: $y_{max}=D/2$, and y_{max} can be substituted into the non-sp curve Eq. (1) to calculate the corresponding x_{max}.

In $\Delta P_{max}O'E$, the Eq. (2) can be established:

$$(R - x_{max})^2 + y_{max}^2 = R^2 . \quad (2)$$

Transforming Eq. (2) gives Eq. (3):

$$R = \left(y_{max}^2 + x_{max}^2\right) / 2x_{max} . \quad (3)$$

Substituting y_{max} and x_{max} into Eq. 3, the size of the nearest circle radius R of the tested component can be calculated;

According to the given non-spherical curve equation, the number of equal segments N can be obtained, and the size of the corresponding equal segment Y value can obtained: y_1, y_2, y_3, …, y_i, then, after the equal value of Y is brought into the Eq. (1), corresponding equal value of X can be calculated: x_1, x_2, x_3, …, x_i, therefore, the coordinate values of the corresponding points P_1, P_2, P_3, …, P_i on the surface curve of the element to be measured can be known.

It can be seen from the relationship of the straight line $O'P_i$ and $O'P_i'$ in Fig. 1 that:

$$P_i'P_i = R - O'P_i . \quad (4)$$

In $\Delta P_iFO'$, the Eq. (5) can be rearranged as:

$$O'P_i = \sqrt{\left(R - x_{p_i}\right)^2 + y_{p_i}^2} . \quad (5)$$

From Eqs. (4) and (5), it can be derived that Eq. (6) is obtained:

$$P_i'P_i = R - \sqrt{\left(R - x_{p_i}\right)^2 + y_{p_i}^2} . \quad (6)$$

The $P_i'P_i$ is the deviation of the non-spherical surface figure from the closest reference sphere.

In $\Delta P_iFO'$, the Eq. (7) can be rearranged as:

$$tan\,\theta_i = \frac{y_{p_i}}{R - x_{p_i}} . \quad (7)$$

Transformation of Eq. (7) gives Eq. (8):

$$\theta_i = arctg\,\frac{y_{p_i}}{R - x_{p_i}} . \quad (8)$$

Substituting the calculated y_1, y_2, y_3, …, y_i and x_1, x_2, x_3, …, x_i into Eq. (8), the angle θ_i corresponding to the deviation $P_i'P_i$ can be calculated.

The obtained values of $P_i'P_i$ and θ_i can be used as the theoretical basis for the detection of non-spherical surface shapes by the nearest method, i.e., placing the vertex of the measured non-spherical curved surface at the endpoint of the nearest circle radius R, the probe of the laser displacement sensor the vertex of the curved surface, and then moving the measured non-spherical surface left or right, the difference between the actual non-spherical curve and the nearest circle can detected. Then, subtracting the obtained difference from the theoretical difference yields the true error value of the non-spherical curve.

3. Design of the Model Structure

Based on the theory of the nearest circle, the small-diameter aspheric surface type detector was designed according to the actual non-spherical aperture demand, shown in Fig. 2. The detector mainly includes: X-axis moving platform, Y-axis moving platform, Z-axis moving platform, moving platform transition frame, torque assembly, rotating shaft, single diaphragm coupling, hub, moving platform connecting elbow plate, laser displacement sensor, sensor connecting elbow plate, bed body assembly, etc.

The laser displacement sensor used in this detector is Keyence LK-H080 series, and its specific technical parameters are as follows: the resolution is 0.01 μm, the linearity is ±0.02% F.S., the measuring range is ±8 mm, and the working distance is 30 mm. This sensor has high frequency response (up to 100 kHz) and anti-environmental light interference capability, which is suitable for high-precision non-contact contour measurement.

Based on the above design, the principal model of the small-caliber non-spherical surface type detector was successfully developed. This model has completed the of the mechanical structure, the integration of the motion control system, and the installation of the laser displacement sensor, and has the basic functions of non-spherical surface type detection, provides a physical platform for the subsequent error compensation and system verification experiments.

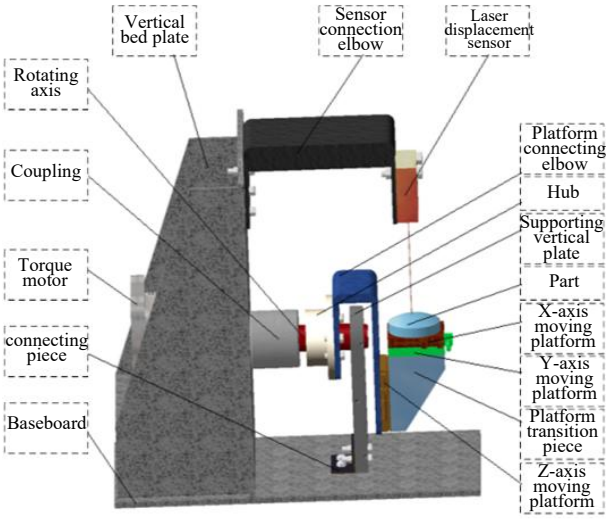

Fig. 2 Schematic diagram of the instrument mechanism structure

4. Geometric Error Compensation Analysis

Up to now, the error types affecting the detection accuracy of the detection instrument are generally considered to include the following: geometric error [9], thermal deformation error [10], force error [11], control system error, etc. [12]. Compared with other errors, the geometric error is the most important one affecting detection accuracy of the detection instrument. Therefore, it is an important link to effectively improve its detection accuracy to carry out geometric error analysis for the principle model.

In this research, the motion axis geometric error is obtained in an incremental form, and the cumulative value is recorded and saved; the incremental error compensation model is established using the cumulative value, and its input is the current position and moving distance of the motion axis, and the output is the error value corresponding to the moving distance of the section the obtained error value is used to implement the lookahead compensation for the moving command, so that the motion axis eliminates it before the error occurs.

4. 1. Establish a database

The measuring shaft is divided equally at any step length, and the error and cumulative value are detected in real time by using a laser interferometer, and the final node cumulative value is calculated by taking the average value of multiple measurements and saved, and its error database ε can be established, as shown in Table 2.

Table 2

The meaning of each parameter in the database

No.	Code	Meaning
1	λ^+, λ^-	Equidistant step length from absolute zero point to positive and negative limits of the test shaft.
2	P_n, P_{-n}	The theoretical position value of the positive and negative limits of the test shaft.
3	P_i, P_{-i}	Theoretical position value between the positive and negative limits of the test shaft.
4	ε_n, ε_i, ε_{-i}, ε_{-n}	The positional error values corresponding to the theoretical position values P_n, P_i, P_{-i} , P_{-n}.

$$\varepsilon = \begin{cases} \varepsilon_n & P_n = n\lambda^+ \\ \vdots & \vdots \\ \varepsilon_i & P_i = i\lambda^+ \\ \vdots & \vdots \\ \varepsilon_1 & P_1 = \lambda^+ \\ 0 & P_0 = 0 \\ \varepsilon_{-1} & P_{-1} = -\lambda^- \\ \vdots & \vdots \\ \varepsilon_{-i} & P_{-i} = -i\lambda^- \\ \vdots & \vdots \\ \varepsilon_{-n} & P_{-n} = -n\lambda^- \end{cases} . \tag{9}$$

4.2. Establish the compensation model

The specific steps for establishing the compensation model are as follows:

Using the two-point straight line method to establish an error approximation straight line between any adjacent node between the absolute zero point and the positive limit of the motion axis, equation is:

$$y = \frac{\varepsilon_{i+1} - \varepsilon_i}{P_{i+1} - P_i} \cdot x + \frac{\varepsilon_i \cdot P_{i+1} - \varepsilon_{i+1} \cdot P_i}{P_{i+1} - P_i} . \tag{10}$$

Similarly, using the two-point straight line method to establish an error approximation straight line between any adjacent node between the absolute zero point of the motion axis and the limit, its equation is:

$$y = \frac{\varepsilon_{-i} - \varepsilon_{-i-1}}{P_{-i} - P_{-i-1}} \cdot x + \frac{\varepsilon_{-i-1} \cdot P_{-i} - \varepsilon_{-i} \cdot P_{-i-1}}{P_{-i} - P_{-i-1}} . \tag{11}$$

Depending on the distribution of the current position P_a and the target position P_b when the motion command is issued by the host computer, the incremental error compensation model can be into the following four cases:

1. $0 \le P_a \le P_n$, $0 \le P_b \le P_n$

Considering that the current position P_a and the target position P_b are both between the absolute zero and the positive limit of the motion axis, the starting position P_a and target position P_b are positioned between the node positions 0-P_n in order of magnitude, assuming $P_i \le P_a \le P_{i+1}$, $P_j \le P_b \le P_{j+1}$ $(0 \le i, j \le n)$, and using the established node approximation equation between the absolute zero and the positive limit, the error values ε_a and ε_b corresponding to the positions P_a and P_b can be obtained, and the formula is as follows:

$$\varepsilon = \frac{\varepsilon \cdot (P - P) - \varepsilon \cdot (P - P)}{P - P} , \tag{12}$$

$$\varepsilon_b = \frac{\varepsilon_{j+1} \cdot (P_b - P_j) - \varepsilon_j \cdot (P_{j+1} - P_b)}{P_{j+1} - P_j} . \tag{13}$$

Then the error value ε' corresponding to the segment move command L is:

$$\varepsilon' = \varepsilon_b - \varepsilon_a \tag{14}$$

Substituting Eqs. (12) and (13) into Eq. (14) yields:

$$\varepsilon' = \frac{\varepsilon_{j+1}\cdot\left(P_b - P_j\right) - \varepsilon_j\cdot\left(P_{j+1} - P_b\right)}{P_{j+1} - P_j} - \frac{\varepsilon_{i+1}\cdot\left(P_a - P_i\right) - \varepsilon_i\cdot\left(P_{i+1} - P_a\right)}{P_{i+1} - P_i} \quad . \tag{15}$$

2. $0 \le P_a \le P_n$, $P_{-n} \le P_b \le 0$

In this case, where the present position P_a is considered to be between the absolute zero and the positive limit of the motion axis, and the target position P_b considered to be between the absolute zero and the negative limit of the motion axis, the starting position P_a is positioned between the node position 0-P_n and the target position P_b positioned between the node position P_{-n}-0, assuming $P_i \le P_a \le P_{i+1}$, $P_{-j-1} \le P_b \le P_{-j}$, the established node approximation equation between the absolute zero and the positive limit and the node approximation equation between the negative limit and the absolute zero, it is possible to obtain the error values ε_a and ε_b corresponding to the positions P_a and P_b, and the formula is as follows:

$$\varepsilon_a = \frac{\varepsilon_{i+1}\cdot\left(P_a - P\right)_i - \varepsilon_i\cdot\left(P_{i+1} - P_a\right)}{P_{i+1} - P_i}, \tag{16}$$

$$\varepsilon_b = \frac{\varepsilon_{-j}\cdot\left(P_b - P_{-j-1}\right) - \varepsilon_{-j-1}\cdot\left(P_{-j} - P_b\right)}{P_{-j} - P_{-j-1}}. \tag{17}$$

Then the corresponding error value of the segment move command L is:

$$\varepsilon' = \varepsilon_b - \varepsilon_a . \tag{18}$$

Substituting Eqs. (16) and (17) into Eq. (18) gives:

$$\varepsilon' = \frac{\varepsilon_{-j}\cdot\left(P_b - P_{-j-1}\right) - \varepsilon_{-j-1}\cdot\left(P_{-j} - P_b\right)}{P_{-j} - P_{-j-1}} - \frac{\varepsilon_{i+1}\cdot\left(P_a - P_i\right) - \varepsilon_i\cdot\left(P_{i+1} - P_a\right)}{P_{i+1} - P_i} \quad . \tag{19}$$

3. $P_{-n} \le P_a \le 0$, $0 \le P_b \le P_n$

In this case, where the present position P_a is considered to be between the absolute zero and negative limit of the motion axis, and the target position P_b is to be between the absolute zero and positive limit of the motion axis, the starting position P_a is positioned between the node positions P_{-n}-0, and the target position P_b is between the node positions 0-P_n, assuming $P_{-i-1} \le P_a \le P_{-i}$, $P_j \le P_b \le P_{j+1}$, using the established approximation equation between the absolute zero and positive limit and the node approximation equation between the negative limit and absolute zero, it is possible to obtain the error values ε_a and ε_b corresponding to the positions P_a and P_b, and the formula is as follows:

$$\varepsilon_a = \frac{\varepsilon_{-i}\cdot\left(P_a - P_{-i-1}\right) - \varepsilon_{-i-1}\cdot\left(P_{-i} - P_a\right)}{P_{-i} - P_{-i-1}}, \tag{20}$$

$$\varepsilon_b = \frac{\varepsilon_{j+1}\cdot\left(P_b - P_j\right) - \varepsilon_j\cdot\left(P_{j+1} - P_b\right)}{P_{j+1} - P_j}. \tag{21}$$

Then the corresponding error value of the segment move command L is:

$$\varepsilon' = \varepsilon_b - \varepsilon_a . \tag{22}$$

Substituting Eqs. (20) and (21) into Eq. (22) gives:

$$\varepsilon' = \frac{\varepsilon_{j+1}\cdot\left(P_b - P_j\right) - \varepsilon_j\cdot\left(P_{j+1} - P_b\right)}{P_{j+1} - P_j} - \frac{\varepsilon_{-i}\cdot\left(P_a - P_{-i-1}\right) - \varepsilon_{-i-1}\cdot\left(P_{-i} - P_a\right)}{P_{-i} - P_{-i-1}} \quad . \tag{23}$$

4. $P_{-n} \le P_a \le 0$, $P_{-n} \le P_b \le 0$

In this case, where the current position P_a is between the absolute zero and negative limit of the motion axis, and the target position P_b is also between the zero and negative limit of the motion axis, both the start position P_a and the target position P_b are positioned between the node positions P_{-n}-0, it is assumed that $P_{-i-1} \le P_a \le P_{-i}$, $P_{-j-1} \le P_b \le P_{-j}$, and the error values ε_a and ε_b corresponding to the positions P_a and P_b can be obtained using the established node approximation equation between the negative limit and the absolute zero, and the formula is as follows:

$$\varepsilon_a = \frac{\varepsilon_{-i}\cdot\left(P_a - P_{-i-1}\right) - \varepsilon_{-i-1}\cdot\left(P_{-i} - P_a\right)}{P_{-i} - P_{-i-1}}, \tag{24}$$

$$\varepsilon_b = \frac{\varepsilon_{-j}\cdot\left(P_b - P_{-j-1}\right) - \varepsilon_{-j-1}\cdot\left(P_{-j} - P_b\right)}{P_{-j} - P_{-j-1}}. \tag{25}$$

Then the corresponding error value of the segment move command L is:

$$\varepsilon' = \varepsilon_b - \varepsilon_a . \tag{26}$$

Substituting Eqs. (24) and (25) into Eq. (26) gives:

$$\varepsilon' = \frac{\varepsilon_{-j}\cdot\left(P_b - P_{-j-1}\right) - \varepsilon_{-j-1}\cdot\left(P_{-j} - P_b\right)}{P_{-j} - P_{-j-1}} - \frac{\varepsilon_{-i}\cdot\left(P_a - P_{-i-1}\right) - \varepsilon_{-i-1}\cdot\left(P_{-i} - P_a\right)}{P_{-i} - P_{-i-1}} \quad . \tag{27}$$

Compensating the current position P_a with the error value ε' obtained, the moving distance L and the target position P_b, the compensated moving command L'' be obtained as shown in the formula (28), i.e. when the upper computer sends the moving command L'', the motion axis can move to the ideal target P_b, thus realizing the geometric error compensation.

$$L'' = L + \varepsilon' . \tag{28}$$

5. Experimental Analysis

To verify the effectiveness of the proposed error compensation method, the experiment of detection and compensation of the motion axis geometric error was carried out on the assembled small-di aspheric surface type measuring instrument. The error compensation experiments of the motion axes X, Y, Z and A are carried out separately according to the error compensation principle described above, as follows.

5.1. Establish a database

Set the equal partition step length λ^+ and λ^- for the establishment of the error database. In order to facilitate the measurement of the error and thus establish the error database, the equal partition step length λ^+ and λ^- of the motion axis X are set to be equal and equal to 10 mm; the partition step length λ^+ and λ^- of the motion axis Y are set to be equal and equal to 10 mm; the equal partition step length λ^+ and λ^- of the motion axis Z are set to be equal and equal to 10 mm; the equal partition step length λ^+ and λ^- of the rotation A are set to be equal and equal to 1°.

In order to accurately describe the size and trend of the error of the motion axis X, Y, Z and A, the number of times N is selected to be equal to 5. Through 5 times of measurement, the average value is taken respectively to establish the final translation axis X Y, Z and A error database, so as to realize the incremental compensation of the error.

5.2. Establish the compensation model

The error of the motion axes X, Y, Z and A obtained above is applied, and the error compensation model between the nodes corresponding to the motion axes X Y, Z and A is established respectively, and the modeling result of the error compensation of the motion axis X is shown in the eq. (29). Here, only the axis X is used as an example to introduce, and the Y axis, Z axis and A axis are basically the same as the X axis.

$$\begin{cases} y = -0.9573x + 1.0227 & [20,30] \\ y = -0.0822x - 16.4787 & [10,20] \\ y = -0.2364x - 14.9373 & [0,10] \\ y = -0.8404x - 14.9373 & [-10,0] \\ y = -0.0278x - 6.8110 & [-20,-10] \\ y = -0.0862x - 7.9790 & [-30,-20] \end{cases} . \tag{29}$$

5.3. Compensation analysis

The error compensation of the motion axes X, Y, Z and A is carried out by applying the error compensation theory studied in the previous text, and the actual data of the error before and after compensation can be obtained, and the error relationship curves before and after compensation of the motion axes X, Y, Z and A are drawn, as in Fig. 3, Fig. 4, Fig. 5, Fig. 6.

It can be seen from the error curve analysis before and after the motion axis compensation of Fig. 3, Fig. 4, Fig. 5, and Fig. 6:

1. The error compensation research carried out for the motion axes X, Y, Z and A can effectively reduce the motion error of the motion axis;

2. Although there are some compensation nodes in the error compensation curve where the compensation effect is slightly large, the overall error compensation effect is very ideal, and the error of the compensated axis fluctuates near the zero line;

3. During the process of building the error compensation model, if the set equal division step length is smaller, the overall error effect will be more accurate.

The error compensation model established by this study has been integrated into the detector control system, and the positioning accuracy of the detector in the actual non-spherical has been effectively improved by real-time

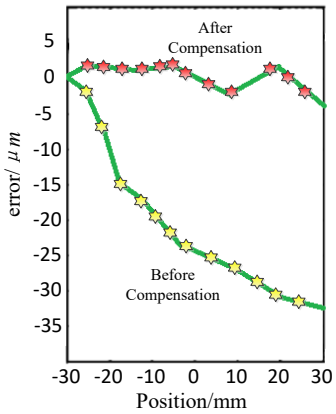

Fig. 3 Comparison of errors before and after X-axis compensation

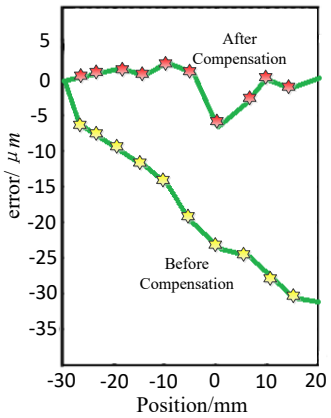

Fig. 4 Comparison of errors before and after Y-axis compensation

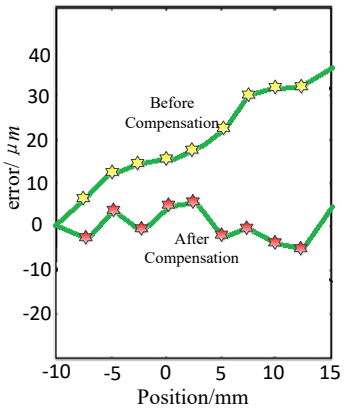

Fig. 5 Comparison of errors before and after Z-axis compensation

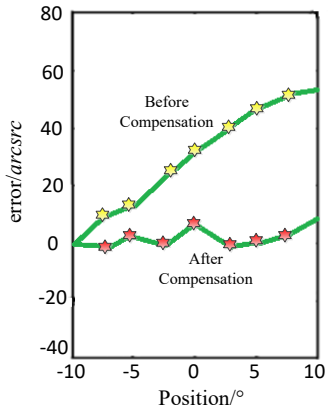

Fig. 6 Error comparison chart before and after compensation of A-axis

look-ahead compensation of the motion command. Subsequent system measurement results show that the compensated detector has the ability of sub-micrometer shape detection.

5.4. System measurement experiments verification

To verify the measurement capability of this detector for actual small-aperture non-spherical elements, a non-spherical mirror with an aperture of Φ10 mm, a vertex curvature radius $R = 20$, and a secondary curve constant $k = -0.8$ was as the object to be measured. The designed surface shape value of this element is known, and it has been calibrated by a Zygo interferometer (Verifire™ MST, and its surface shape error peak PV ≤ 0.1 μm.

The calibrated non-spherical mirror is installed on the rotating shaft of the detector, and laser displacement sensor is adjusted to aim at the vertex of the element. According to the steps described in Section 2.2, $N = 100$ points are equally divided the Y direction, and the actual contour and the deviation value from the nearest circle are collected point by point, and converted into surface shape height data.

In order to quantify the accuracy, the detector's measurement results are compared with those of the Zygo interferometer, and the root mean square (RMS) of the surface shape error is calculated be 0.015, and the peak (PV) is 0.08 μm. Repeated measurements 5 times, the standard deviation of the RMS the surface shape obtained is 0.018 μm, indicating that the detector has good repeatability.

The above experimental results show that this detector can achieve high- measurement of the surface shape of small-aperture non-spherical elements, and its measurement results agree well with the interferometric measurement values, which verifies the effectiveness the proposed detection principle and error compensation method.

6. Conclusions

1. The structural design research of a new type of aspheric surface profile measuring instrument was carried out, the aspheric surface profile measuring based on the nearest circle method was analyzed, the comprehensive analysis of the error source of the aspheric surface profile measuring instrument was completed, and the spatial comprehensive error model of the asp surface profile measuring instrument was established based on the multi-body system kinematics theory and the principle of homogeneous coordinate transformation.

2. The error testing technology analysis of the aspheric profile measuring instrument was carried out, the spatial geometric error detection of the moving axis of the aspheric surface profile measuring instrument was carried out by using the laser interferometer, the error implementation scheme of the aspheric surface profile measuring instrument was proposed, the error compensation model was established, and the effectiveness of this research content was verified by experiments, which effectively improved the profile detection accuracy of the aspheric surface.

3. Aiming at the problems of insufficient accuracy and other issues in traditional detection technology, this research proposes an opto-mechatronics solution based on the nearest-circle method. The results of systematic measurement experiments show that the surface shape error RMS of the measuring instrument is 0.015 μm the PV value is 0.08 μm, and the repeatability standard deviation is 0.018 μm. It has good engineering application prospects. The results provide theoretical support and technical paths for the independent research and development of domestic high-end optical detection equipment, and can effectively promote the large-scale application of aspheric elements consumer electronics, autonomous driving and other fields. It has certain engineering significance for enhancing the competitiveness of China's optical manufacturing.

Acknowledgments

This work was supported by the Science and Technology Plan Project of Chengde City (No. 202201A061) and the Program of Free Exploration of the Department of Science and Technology of Jilin Province (No. YDZJ202201ZYTS391).

References

1. **Zhang, T.; Chen, D.; Yang, H.; Zhao, W.; Wang, Y.; Zhou, H.** 2024. Spreading Behavior of Non-Spherical Particles with Reconstructed Shapes Using Discrete Element Method in Additive Manufacturing, Polymers 16(9): 1179. https://doi.org/10.3390/POLYM16091179.
2. **Qian, Y. C.; Cai, R. R.; Zhang, L. Z.** 2023. A spheropolyhedral-based discrete element lattice Boltzmann method for simulation of non-spherical adhesive particulate flow, Computer Physics Communications 291: 108809. https://doi.org/10.1016/J.CPC.2023.108809.
3. **Alzahrani, A.; Alsulami, T.; Salamatullah, A. M.; Ahmed, S. R.** 2023. Non-spherical gold nanoparticles enhanced fluorescence of carbon dots for norovirus-like particles detection, Journal of Biological Engineering 17(1): 33. https://doi.org/10.1186/S13036-023-00351-X.
4. **Loizeau, N.; Farrar, G. R.** 2022. Non-spherical dark matter structures detection, Journal of Cosmology and Astroparticle Physics 2022: 049. https://doi.org/10.1088/1475-7516/2022/03/049.
5. **Chen, X.; Chen, Y. C.; Yu, W.; Hu, S. M.; Li, P. C.** 2025. Noncontact elastography of soft material using a laser profilometer with airpuff excitation, Mechanical Systems and Signal Processing 228: 112465.

https://doi.org/10.1016/J.YMSSP.2025.112465.
6. **Sun, Y. J.; Zhou, W. Y.; Liu, Z. W.; Li, W. H.; Jiang, S.; Liu, L.; Jiang, Y. X.; Wang, W. C.** 2025. Large-format grating groove density measurement method based on optical interferometry, Optics and Lasers in Engineering 187: 108885. https://doi.org/10.1016/J.OPTLASENG.2025.108885.
7. **Ma, T. Y.; Wei, Q. Y.; Lyu, Z. L.; Zhang, D. B.; Zhang, H. Y.; Wang, R.; Dong, J. H.; Liu, Y. Q.; Yao, R. T.; He, Z. X.** 2021. Self-Collimating SPECT With Multi-Layer Interspaced Mosaic Detectors, IEEE Transactions on Medical Imaging 40(8): 2152-2169. https://doi.org/10.1109/TMI.2021.3073288.
8. **Stark, C. R.; Diver, D. A.; Swayne, M. I.** 2025. Electrostatic instability of non-spherical dust in sub-stellar clouds, Plasma Physics and Controlled Fusion 67(2): 025016. https://doi.org/10.1088/1361-6587/ADA1FB.
9. **Caucao, S.; Gatica, N. G.; Gatica, F. L.** 2025. A posteriori error analysis of a mixed finite element method for the stationary convective Brinkman–Forchheimer problem, Applied Numerical Mathematics 211: 158-178. https://doi.org/10.1016/J.APNUM.2025.01.007.
10. **Li, Y.; Chen, X.; Liu, G. S.; Rao, P.** 2025. Correction Method for Thermal Deformation Line-of-Sight Errors of Low-Orbit Optical Payloads Under Unstable Illumination Conditions, Remote Sensing 17(5): 762. https://doi.org/10.3390/RS17050762.
11. **Zhang, S. H.; Li, Y.; Che, L. Z.; Tian, W. H.** 2023. A new integrated model of deformation resistance and its application in prediction of rolling force of a thick plate, Journal of Iron and Steel Research International 31(4): 882-893. https://doi.org/10.1007/S42243-023-01084-3.
12. **Cavanini, L.; Felicetti, R.; Ferracuti, F.; Monteriù, M.** 2024. Error governor for active fault tolerance in PID control of MIMO systems, International Journal of Systems Science 56(7): 1457-1473. https://doi.org/10.1080/00207721.2024.2427850.

Y. Li, Y. Hu, B. Yu

THE STRUCTURE DESIGN AND PRECISION IMPROVEMENT OF SMALL CALIBER NON-SPHERICAL SURFACE TYPE DETECTOR

S u m m a r y

Aspherical optical elements have significant advantages over traditional spherical elements, and have become the core technology for high-resolution imaging, intelligent devices, and precision instrument upgrades through optical performance, simplifying system structure, and reducing manufacturing costs. It has gradually promoted the development of optical systems towards high performance, lightweight, and high quality. However, the rapid development of aspheric optical elements is limited by the detection technology of aspheric surface profile. In order to solve the problems of detection principle error, low detection efficiency, expensive detection instruments and poor general performance in the current non-spherical optical elements shape detection technology, a new principle of non-spherical surface shape detection is proposed based on the theory of the closest circle, and the detection numerical model of non-spherical is constructed. At the same time, based on this, the overall structure design of small aperture non-spherical surface shape detection instrument is carried out, and the specific steps of detection instrument to implement small aperture non-spherical surface shape detection are analyzed. In order to further improve the detection accuracy of the small-caliber non-spherical surface profile detector, the detection technology of the geometric error of the is studied. The spatial geometric error detection of the moving axis of the small-caliber non-spherical surface profile detector is carried out by using the laser interferometer, and the compensation scheme of the small-caliber non-spherical surface profile detector is proposed through the analysis of the error compensation logic. In addition, the mathematical model of geometric error is established. The correctness of the research content is effectively verified by carrying out the geometric error compensation experiment on the moving axis of the small-caliber non-spherical surface profile, and the research on the accuracy improvement of the small-caliber non-spherical surface profile detector is completed.

Keywords: small-caliber aspheric, surface shape detection, precision improvement, error compensation.

Received July 5, 2025
Accepted February 20, 2026